Open Ceramics 10 (2022) 100249

Contents lists available at ScienceDirect

Open Ceramics

journal homepage: www.sciencedirect.com/journal/open-ceramics

Improving the frost resistance of roof tiles beyond current prediction schemes

Chiara Zanelli [a,*], Dircetti Girolamo [b], Conte Sonia [a], Molinari Chiara [a], Dondi Michele [a]

[a] CNR-ISTEC, Institute of Science and Technology for Ceramics, Faenza, Italy
[b] ECAM-RICERT srl, Monte di Malo, Italy

ARTICLE INFO

Keywords:
Durability
Frost resistance
Mechanical strength
Pore size distribution
Roof tile

ABSTRACT

Frost resistance is an important requirement for clay roof tiles and the most difficult to keep under control during industrial production. Durability under freeze/thaw cycles is related with the capillary pore system, and current models predict the lower the open porosity and the coarser the pore size, the better the frost resistance. This implies, however, high firing temperature and rather refractory clay bodies, which are in contrast with energy and resource efficiency. Therefore, a different approach is needed to improve frost resistance of roof tiles without stressing the concept of low porosity and coarse pore size. A case-study is presented to demonstrate how excellent frost resistance can be achieved by adjusting raw materials formulation and firing schedule. Raw materials and bodies were characterized by XRF, ASTM C958 and technological properties. Both laboratory tests were performed: the products were characterized by water absorption (ASTM C67), open porosity and pore size distribution (Hg porosimetry), phase composition (XRD-Rietveld), mechanical strength (EN 538) and frost resistance (EN 539-2) up to 400 freeze/thaw cycles. Durability of roof tiles was drastically improved acting on both pore size distribution (eliminating pores <0.1 μm) and increasing mechanical strength (>13 MPa). Phase composition plays a complex role with opposite effects of new formed phases versus amorphous phase and residual clay minerals. A satisfactory target (no damages after 250 freeze/thaw cycles) was achieved firing at 900 °C (7% pores <0.1 μm) while the best performance (no damages after 400 cycles) required firing at 950 °C (<1% pores <0.1 μm). Excellent frost resistance (well beyond the standard 50 cycles) can be obtained through proper design of firing schedule and body composition, even for temperatures below 950 °C.

1. Introduction

Frost resistance is the most important factor affecting roof tiles durability in cold and temperate climates. The prolonged action of freezing and thawing leads to the formation of micro-cracks that can bring about further damages, which are somehow related to the extent of water saturation of the ceramic material, as well as its amount of porosity and pore size [1–7].

The concept underneath these observations is that frost damage can be tolerable below critical values of pore dimensions and open porosity. This led several authors to elaborate empirical models that predict the frost resistance on the basis of the porous microstructure of roof tiles [2,8–17]. Such models consist of equations that calculate a frost resistance index from one or more parameters that must be experimentally determined: water absorption (in different experimental conditions), capillary coefficient, amount and size of pores, amongst others. However, criticism about the applicability of these models has emerged, as in many cases the results are not fully consistent with the frost behavior of roof tiles under operating conditions [5,18,19].

Nevertheless, an advantage of these models is that they are based on variables of technological significance, which are dependent on process parameters – like the firing schedule [20–24] – or on the body composition [5,22,25–27]. As a consequence, the industrial design of frost-resistant roof tiles is mainly based on the concept behind these models: the coarser the pore size and the smaller the open porosity, the better the frost resistance.

Such a concept, however, when applied uncritically to improve the durability of roof tiles, tends to push towards increasingly high firing temperatures (peaking at 1050–1100 °C in industrial production) which are known to promote a pore coarsening effect [6,23,24]. This is clearly in contrast with the general objectives of energy saving and reduction of CO_2 footprint of the ceramic industry [28] which can be achieved by

* Corresponding author.
E-mail address: chiara.zanelli@istec.cnr.it (C. Zanelli).

https://doi.org/10.1016/j.oceram.2022.100249
Received 27 December 2021; Accepted 17 March 2022
Available online 8 April 2022

reducing consistently the peak firing temperatures [29]. The implicit limitation in using the aforementioned models as primary tools for predicting frost resistance can only be circumvented through a broader analysis of the physical and compositional properties of materials [5] and including further variables, like mechanical strength [6,17,30,31].

The goal of the present study is to demonstrate that it is possible to produce roof tiles with an excellent frost resistance but firing at relatively low temperature (i.e., below 960 °C). The rationale consists in changing body composition and firing temperature – in order to get a range of microstructural, compositional and mechanical properties of roof tiles – then determine frost resistance to reveal the best performance. The underlying strategy is by mix design with firing in the 850–950 °C range and through a series of long-lasting freeze-thaw cycles.

2. Experimental

Roof tiles have an added value high enough, at variance of other heavy-clay products, to benefit from clay sources also quite distant from the plant. In our case, bodies comprise two different types of clays from Coppette quarry, Santena, Turin, Piedmont (P) and Braglie quarry, Carpineti, Reggio Emilia, Emilia-Romagna (S) respectively. Clay P was extracted from Pleistocene fluvio-glacial deposits [32] while clay S from the Eocene-Oligocene Montepiano Formation [33]. Batch formulation combined clay P with increasing amount of clay S by weight in the bodies, which are named A (5% S + 95% P), B (15% S + 85% P) and C (25% S + 75% P). Raw materials and bodies were analysed for chemical (XRF, ASTM 1605-04), particle size distribution (ASTM C958, Micromeritics Sedigraph 5100) and methylene blue index (EN 933-9).

Laboratory simulation of the industrial tilemaking cycle consisted of body preparation (mixing, moisturing, pan milling), extrusion under vacuum (tiles 20 × 10 × 2 cm), drying (in chamber drier) and firing in electric chamber kiln (heating rate 50 °C per hour up to 850, 900 or 950 °C, 8 h dwell time). Technological properties of semi-finished products were determined: working moisture (CEN ISO/TS 17892-1), drying and firing shrinkage (ASTM C326), dry bending strength (EN 10545-4).

Finished products were characterized by determining: frost resistance (EN 539-2), water absorption and saturation coefficient (ASTM C67), open porosity and pore size distribution (mercury intrusion porosimetry, Themo Finnigan Pascal 140, UK), phase composition (X-ray Powder Diffraction, Bruker, D8 Advanced with LynxEye detector, Germany), and mechanical strength (EN 538).

Frost resistance was determined in a climatic chamber (model VBT 03/1000/S, Votsch Industrie-technik, Germany) by a severe procedure: 30 tiles for every sample underwent up to 400 freeze/thaw cycles (instead of 50 cycles prescribed by the standard EN 539-2) going from +15 °C to −15 °C with defrosting by water immersion. As the test proceeded, the tiles could be affected by defects typical of the action of frost, such as cracks perpendicular to the main face of the specimens (that eventually grew until the tile rupture); cracks parallel to the main face (delamination) which ultimately lead to detachment of material (exfoliation); disintegration of parts that turned out to be friable (crumbling). The onset of any flaw led to the classification as a defective specimen, which was no longer subjected to further testing. Frost resistance is expressed in two ways: as the percentage of flawless specimens after every 50 freeze/thaw cycles, and as an index (FR) calculated attributing one point each cycle passed without defects by every tile, normalized for the maximum value achievable (400 cycles and 100% flawless tiles).

Porosimetric data were interpreted according to Fig. 1, particularly parameters required by prediction schemes (total pore volume, median pore diameter, fraction of pores larger than 3 μm). In addition, two main pore populations were found and named 1 and 2 – over and below 0.1 μm, respectively – which pore mode and relative pore volume percentage were determined.

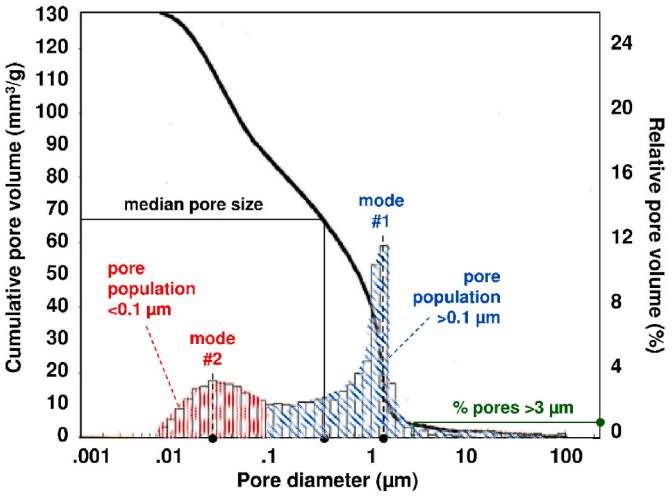

Fig. 1. Mercury intrusion porosimetry plot illustrating how the various parameters were calculated.

The phase composition was determined by using X-ray powder diffraction (in the 5–80° 2θ range, with a point detector equivalent time of 185 s per 0.02° 2θ scan step (D8 Advance equipped with LynxEye detector, Bruker, Germany) on the powdered samples admixed with 20% corundum as the internal standard in order to quantify the amorphous phase. The quantitative interpretation of the patterns was carried out using RIR-Rietveld refinement (GSAS-EXPGUI software package 2001); the experimental error was within 5% relative [34] and an example is given in Fig. 2.

3. Results

3.1. Chemical composition and technological behaviour of the obtained bodies

The two clays P and S exhibit a quite similar chemical composition (Table 1) even if the SiO_2/Al_2O_3 ratio of clay P (2.8) is lower than the ratio of clay S (3.4). Further differences concern the particle size distribution: clay S is remarkably finer than clay P, as attested by a more abundant fraction <2 μm (51% vs. 30%) and only 11% of fraction >20 μm against 40% of clay P (Fig. 3). Both composition and particle size of

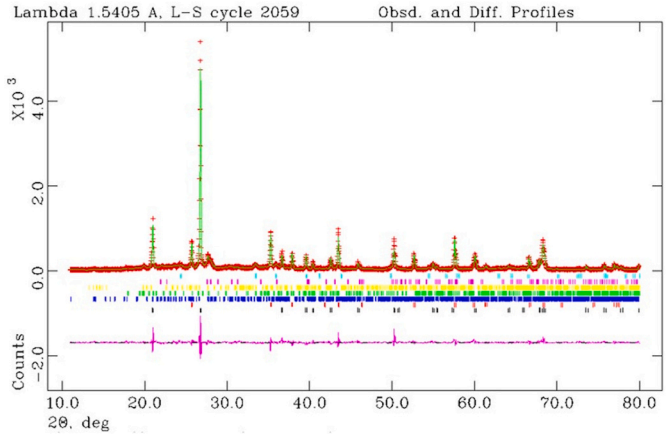

Fig. 2. Example plot of Rietveld refinement performed on X-ray powder diffraction data. The experimental data are indicated by plus signs, the calculated pattern is the continuous line and the lower curve is the weighted difference between the calculated and observed patterns. The rows of vertical tick marks shows the allowed reflections for the crystalline phases present in the sample.

Table 1
Chemical composition, particle size and technological behavior of clays P and S, and bodies A-B-C.

Clay or body	Unit	P	A	B	C	S	e.u.
Percentage of clay S in the batch		0%	5%	15%	25%	100%	
SiO_2	%wt	54.8	55.0	55.3	55.7	58.2	0.8
TiO_2	%wt	1.2	1.2	1.1	1.1	0.8	<0.1
Al_2O_3	%wt	19.8	19.7	19.4	19.2	17.4	0.3
Fe_2O_3	%wt	9.2	9.1	8.9	8.7	7.2	0.2
MgO	%wt	3.0	3.0	3.0	3.1	3.2	0.1
CaO	%wt	0.8	0.8	0.9	1.0	1.4	0.1
Na_2O	%wt	0.6	0.5	0.6	0.6	0.5	<0.1
K_2O	%wt	2.9	2.9	3.0	3.1	3.5	0.1
L.o.I. 1050 °C	%wt	7.5	7.5	7.5	7.5	7.4	0.1
Particle fraction >20 μm	%wt	40	30	29	27	11	1
Particle fraction 2–20 um	%wt	30	38	37	35	38	1
Particle fraction <2 μm	%wt	30	33	35	38	51	1
Methylene Blue index	mL	28	32	36	39	72	1
Working moisture	%wt	18.8	19.2	19.3	19.9	23.0	0.2
Dry bending strength	MPa	7.4	7.7	8.3	9.2	13.7	0.5
Drying shrinkage	cm/m	5.3	5.4	5.5	5.7	6.8	0.1
Firing shrinkage at 850 °C	cm/m	−0.1	−0.1	0.1	0.1	0.9	0.1
Firing shrinkage at 900 °C	cm/m	0.1	0.1	0.3	0.4	1.6	0.1
Firing shrinkage at 950 °C	cm/m	0.5	0.6	0.8	0.9	2.1	0.1

e.u. = experimental uncertainty.

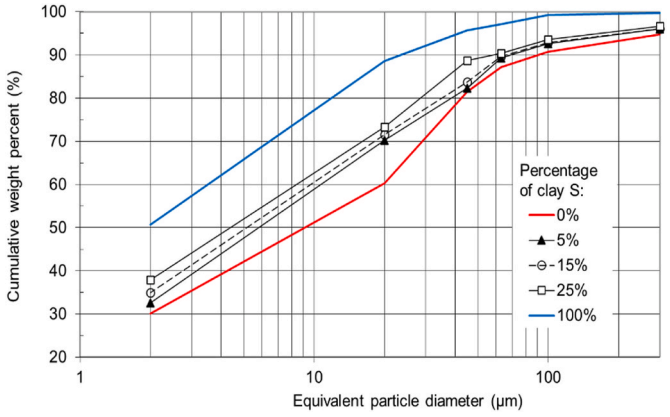

Fig. 3. Particle size distribution of clays and bodies.

mixtures A, B and C are proportional to the P-to-S clay ratios.

Although differences between batches A, B and C appear to be modest, they have a significant repercussion on the technological behavior. Indeed, plasticity (methylene blue index) and working moisture increased moving from batch A to C, consequently causing a growth of drying shrinkage and especially the dry bending strength. Also, the firing shrinkage increased at every peak temperature (Table 1). All these variations are within the acceptance window in the clay roof tile industrial practice.

3.2. Technical performance of roof tiles

The porosity and mechanical resistance of roof tiles vary upon the batch composition and firing schedule (Table 2). Such a matrix 'batch formulation x firing temperature' gives rise to a range of values for water absorption (7.5–13% in cold water), saturation coefficient (0.67–0.86), and bending strength (5–15 MPa). Water absorption is increased as clay S decreased (batches C-B-A) and for lower firing temperatures. On the contrary, the mechanical resistance increased with the peak temperature and amount of clay S (batches A-B-C). In other words, the finer and more plastic the clay batch, the greater the flexural strength and the lower the porosity of roof tiles.

3.3. Pore structure

We found that the pore structure of the roof tiles changed according to the mix design and mainly with the firing temperature. A general trend is evident with distinct evolution of the two pore populations with increasing peak temperature in the range from 850 to 950 °C. (Fig. 4). A progressive decrease of the pores volume below 0.1 μm (population #2) was observed, until nearly disappearing at 950 °C in the body C, along with a moderate pore coarsening (Table 3). The complementary pore population #1 (above 0.1 μm) increased its relative percentage and was characterized by an evident pore coarsening, with mode going from ~1 μm (850 °C) to 2.4–2.8 μm (950 °C). The amount of the coarsest pores (>3 μm) grew from 1 to 3% (850 °C) to 6–11% (950 °C) in volume.

The Maage's durability factor is found to grow by increasing the firing temperature. This can be ascribed to co-existing phenomena: decrease of the pore volume and increase of the pore fraction >3 μm (Table 3). In contrast, the trends as a function of the amount of clay S are not systematic: the Maage's factor increased with the S percentage after firing at 950 °C, but it decreased at 900 °C and varied a little at 850 °C.

3.4. Phase composition

The phase composition of roof tiles shows a certain variability depending on both the amount of clay S and the firing temperature (Table 4). We found that samples are mainly made of quartz and amorphous phase, ranging from 30% to 39% and from 24% to 57%, respectively. In addition, illite/mica occurred up to 28% but tends to disappear with the temperature increase. We also found plagioclase and K-feldspar (both from 2% to 15%).

As expected, increasing the firing temperature led to a gradual decomposition of illite/mica and parallel increase of the amorphous phase content in batches A and B. An opposite trend is shown by batch C (25% clay S) since a significant amount of micaceous mineral is still present after firing at 950 °C and consequently the amorphous phase did not increase. Residual phases are mostly represented, along with illite/mica, by quartz that was substantially stable in the thermal range

Table 2
Technical properties of roof tiles obtained with batches A-B-C fired at different temperatures.

Property	unit	A85	A90	A95	B85	B90	B95	C85	C90	C95	e.u.
Firing temperature	°C	850	900	950	850	900	950	850	900	950	5
Bending strength	MPa	5.4	11.8	12.0	7.7	14.2	13.9	9.5	14.3	14.9	0.8
Water absorption (1)	%wt	13.0	11.6	9.5	11.6	9.7	8.3	11.5	9.5	7.5	0.1
Water absorption (2)	%wt	15.2	14.3	13.0	13.5	12.7	11.9	13.3	12.5	11.2	0.1
Saturation coefficient	1	0.86	0.81	0.73	0.86	0.76	0.70	0.86	0.76	0.67	0.01

[1] water at room temperature for 24 h.
[2] boiling water for 5 h; e.u. = experimental uncertainty.

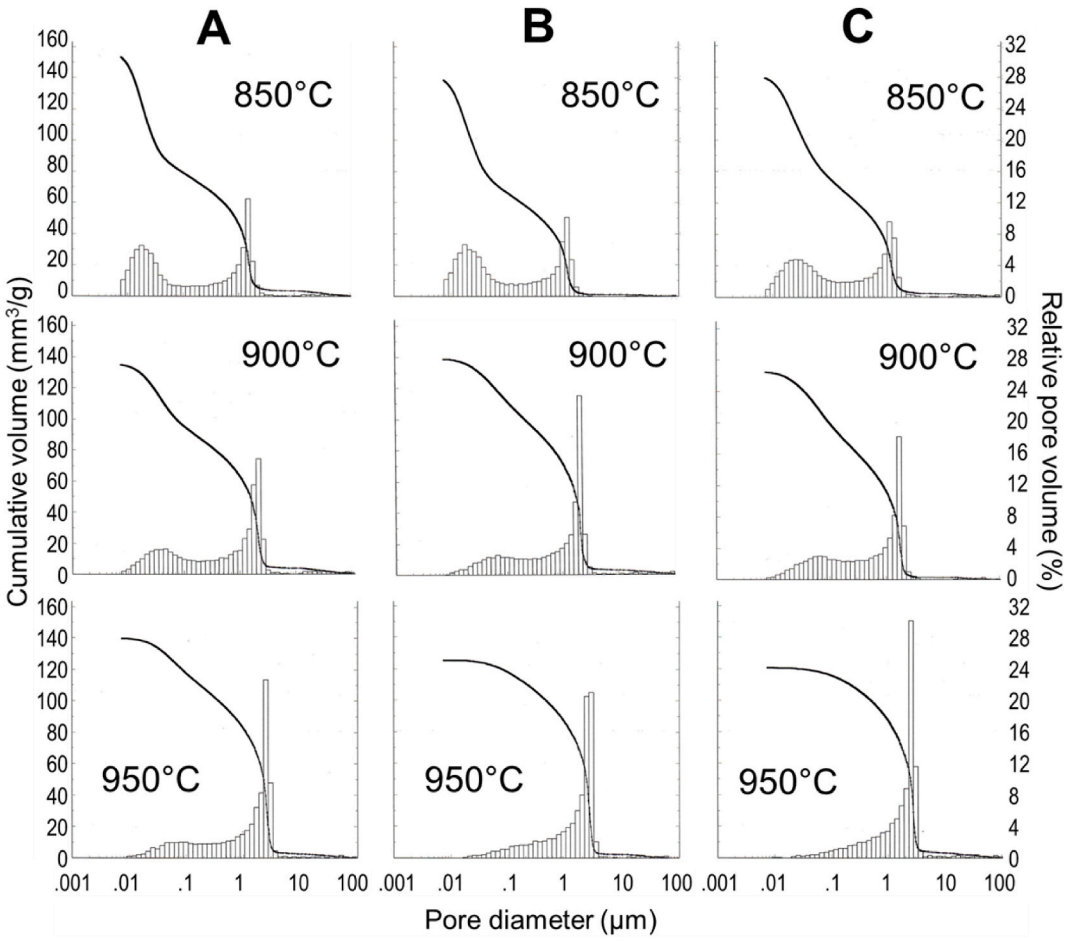

Fig. 4. Mercury intrusion porosimetry graphs of bodies A-B-C fired at 850, 900 or 950 °C.

Table 3
Porosimetric characteristics and durability factor of roof tiles.

Property	unit	A85	A90	A95	B85	B90	B95	C85	C90	C95	e.u.
Open porosity	%vol	29.1	27.1	28.0	26.5	27.9	24.3	28.0	25.9	24.2	0.2
Bulk density	g·cm^{-3}	1.898	2.011	2.009	1.911	2.006	1.935	2.005	1.956	2.009	0.002
Median pore diameter	μm	0.10	0.18	1.40	0.08	1.00	1.95	0.14	0.17	2.00	0.02
Pore mode #1	μm	1.04	2.00	2.40	1.05	2.00	2.80	1.00	1.06	2.70	0.05
Pore mode #2	μm	0.018	0.035	0.090	0.017	0.070	—	0.024	0.065	—	0.003
Pores >3 μm	%vol	2.9	4.2	5.9	1.0	3.2	7.0	2.3	1.9	10.4	0.5
Pores 0.1–3 μm	%vol	13.2	13.2	15.2	11.6	18.0	13.6	12.4	16.6	12.9	0.5
Pores <0.1 μm	%vol	13.0	9.7	6.9	13.9	6.7	3.7	13.3	7.4	0.9	0.5
Maage's durability	1	27.8	33.8	37.1	25.5	30.7	42.3	28.5	28.7	51.5	0.5

e.u. = experimental uncertainty.

Table 4
Phase composition of fired roof tiles (experimental uncertainty ±1%).

Phase (%wt)	A85	A90	A95	B85	B90	B95	C85	C90	C95
Quartz	39	39	34	33	35	35	30	33	37
Illite/mica	28	13	<1	15	11	<1	27	24	15
K-Feldspar	2	4	3	15	13	3	6	6	14
Plagioclase	2	4	4	6	8	15	4	10	7
Hematite	<1	4	2	<1	<1	2	3	3	3
Amorphous phase	29	36	57	31	33	45	30	24	24

considered. Feldspars are partly inherited from clays, where they are present in small amounts, and partly formed during firing. There are clues that K-feldspar formed from illite/mica breakdown, while plagioclase from calcite decomposition, even though they exhibit different trends with temperature in the three series.

3.5. Frost resistance

The roof tiles were in some cases damaged due to freeze-thaw cycles. The typical effects of frost are illustrated in Fig. 5 and consist of the appearance of cracks, delamination, exfoliation, crumbling, or rupture.

The onset of such defects is a probabilistic phenomenon, which has been quantified by the percentage of flawless specimens after every 50 cycles (Fig. 6). Although all batches passed the threshold imposed by the EN standard (50 freeze/thaw cycles) – the behaviour of the various bodies was different according to the clay composition and the firing temperature.

No tiles fired at 850 °C exceeded 150 cycles without rupture, while on average 87% of tiles fired at 950 °C withstood 400 cycles. Samples fired at 900 °C exhibit a marked difference depending on the clay mixture: body A90 did not resist beyond 300 cycles, whereas 67%–94% of tiles C and B, respectively, had no damage after 400 cycles.

However, there is no constant order of frost resistance for the different clay ratios: at 850 °C sample A is the most performing, even though at 900 °C and 950 °C it is the B mixture to be slightly better than mix C (Fig. 7).

Interestingly, the mechanical strength of intact tiles did not change significantly after freeze-thaw cycles. No frost-damaged specimen was tested, of course. Indeed, the flexural modulus of rupture always remains comparable to the value of the material not subjected to frost within 2 times the standard deviation of data (Table 5). A clue of damaging may be seen for some samples in the higher standard deviation of data occurring after a large number of freeze-thaw cycles.

4. Discussion

Different microstructures of roof tiles were obtained by mix design (admixing P and S clays in various ratios to get the A-B-C batches) and varying the firing temperature (850, 900 or 950 °C) despite the a quite similar chemical composition of unfired bodies. By analysing the obtained results, the following observations can be done.

The finer and the more plastic were the batches, the greater the flexural strength and the lower the porosity were in fired roof tiles, as usually found in the industrial practice [22,35,36]. The mechanical strength of roof tiles after freeze-thaw cycles remained comparable to the material not subjected to frost.

The Maage's durability factor increased (from 25 up to 52) with the firing temperature due to both the decrease of pore volume and the increase of the pore fraction >3 μm. A first observation regards the threshold of DF = 50 or 70 that is indicated to have a high probability for the material to be frost resistant in severe climate conditions [9,10]. However, our data demonstrate, even with values of DF as low as 28, that roof tiles can have a good frost resistance (i.e., passing 200 freeze-thaw cycles) while excellent frost performance (at least 90% of roof tiles passing 400 freeze-thaw cycles) was found for DF from 30 to 52. This confirms what some authors have already found about empirical models, like the Maage's approach: caution is necessary in their application since in many cases results may be not consistent. Indeed, some properties strictly depend on the behaviour of the material under real working conditions [5,18,19,21,23,30,31,37].

Excellent frost resistance was obtained, with a clear dependence on the firing temperature (on average 87% of tiles fired at 950 °C withstood 400 freeze-thaw cycles, and 100% in case of batch B95). In our case, changing the body composition and the firing temperature, roof tiles with varying properties are obtained in terms of both microstructure (size and quantity of pores) and phase composition with repercussion on the mechanical properties (Fig. 8).

Frost resistance shows a rather close dependence on the pore size distribution: while the relationship with the extent of large pores is consistent with the Maage's model (Fig. 8a), an even closer relationship emerges with the amount of pores <0.1 μm, suggesting that such tiny porosity is detrimental for the frost resistance (Fig. 8b). This leads to the conclusion that the smaller the amount of micropores (<0.1 μm) and the greater the coarse porosity (>3 μm) the better the durability of the tiles [5,18,19,25].

A clear dependence between the phase composition and the frost resistance is not evident; opposite effects are observed between new formed phases versus amorphous phase and the residual clay minerals (Fig. 8c). Only for batches C, it can be observed that the ratio of new formed phases versus amorphous phase and the residual clay minerals leads to an increase in the durability of the roof tiles [21–23].

The mechanical strength exhibits a good correlation with the frost resistance and the durability of the roof tiles, values than 13 MPa are associated excellent frost resistance index (i.e. > 85).

The durability of roof tiles is improved by acting on the mix design and firing temperature. Indeed, products with satisfactory frost resistance are obtained even at a firing temperature of 900 °C, while the best performance is at 950 °C (Fig. 8d) as already raised in the literature [37]. Therefore, modelling of frost resistance must consider several correlated factors, including the behaviour of the ceramic matrix during the production process (particularly the changes in microstructure and phase composition with firing temperature).

5. Conclusions

Frost-resistant roof tiles are currently designed trying to minimize water absorption and have a pore size distribution as coarse as possible. This implies the choice of batch compositions and firing schedules in open contrast to the pillars of sustainability, i.e., resource efficiency and reduction of energy consumption. In fact, this approach brings about a limited use of local raw materials (since they often do not match with the low water absorption requirement) and a high firing temperature (to get

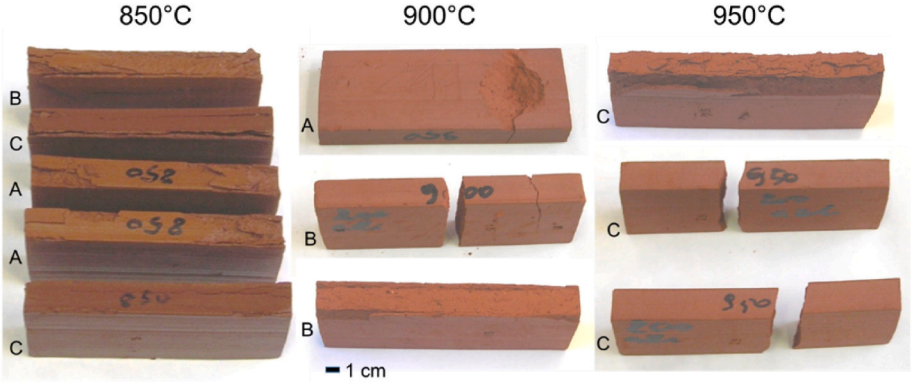

Fig. 5. Types of defects occurring after freeze-thaw cycles in bodies A-B-C fired at 850, 900 or 950 °C, including cracks, delamination, exfoliation, crumbling, rupture.

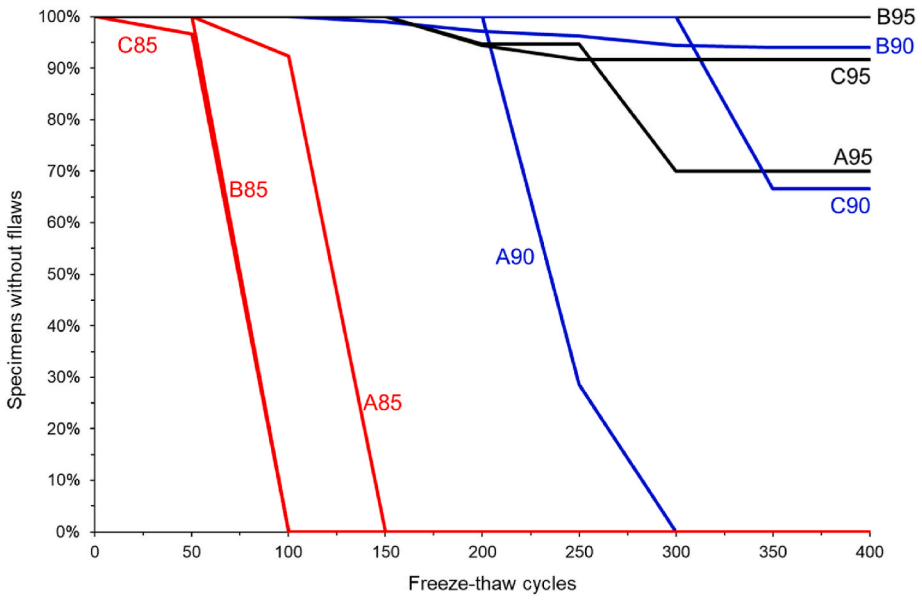

Fig. 6. Percentage of flawless specimens as a function of freeze/thaw cycles.

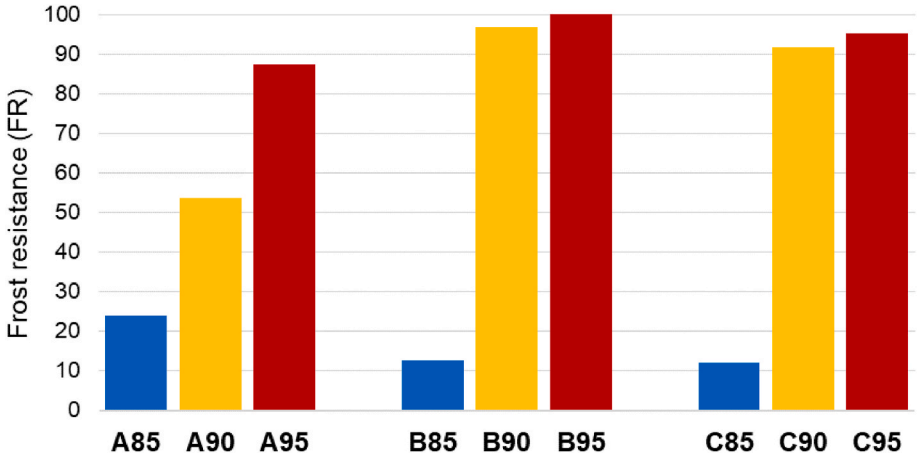

Fig. 7. Frost resistance index (FR) of the roof tiles.

Table 5
Flexural modulus of rupture of flawless roof tiles before (0 cycles) and after freeze-thaw cycles (from 50 to 350). Data are expressed in MPa as mean value (m) and standard deviation (sd).

cycles	0		50		100		150		200		250		300		350	
	m	*sd*	m	*sd*	m	*sd*	m	*sd*	m	*sd*	m	*sd*	m	*sd*	m	*sd*
A85	5.4	0.7	5.5	0.7	5.0	1.5	6.0	1.2								
A90	11.8	0.5	11.8	0.8	11.9	0.5	12.0	0.5	12.2	1.3	11.8	0.7	11.1	1.4		
A95	12.0	0.4	12.3	0.3	12.7	0.3	13.3	0.8	12.8	0.6	12.8	0.8	12.3	0.9	12.7	1.4
B85	7.7	0.8	6.4	0.8	5.7	0.6										
B90	14.2	0.5	13.6	0.4	13.6	0.4	13.4	0.7	13.8	0.5	12.5	0.8	14.0	0.9	14.5	0.4
B95	13.9	0.7	13.8	0.7	13.8	0.7	13.9	1.1	14.5	0.9	14.6	0.5	14.5	0.7	14.8	0.9
C85	9.5	0.7	9.5	2.9	10.2	2.4										
C90	14.3	0.6	15.1	0.8	14.3	0.5	14.5	0.5	15.2	0.8	15.5	0.8	15.1	0.4	15.2	1.0
C95	14.9	0.4	15.6	0.3	16.0	0.7	15.5	0.7	16.0	0.6	16.4	0.7	16.0	0.8	16.3	1.4

a coarse pore size distribution, which means over 1000 °C and in some cases approaching 1100 °C).

The aim of this research was to assess whether it is possible or not to make roof tiles with excellent frost resistance even in conditions far from those imposed by the aforementioned microstructural model. Therefore, a range of microstructures was studied, obtained with batch compositions and firing temperatures that are affordable for tile manufacturers. Analysing the results, it emerged that:

- It is possible to obtain a high frost resistance by firing between 900 and 950 °C (that is a moderate temperature with respect to the industrial practice, where the same target is obtained above 1000 °C);

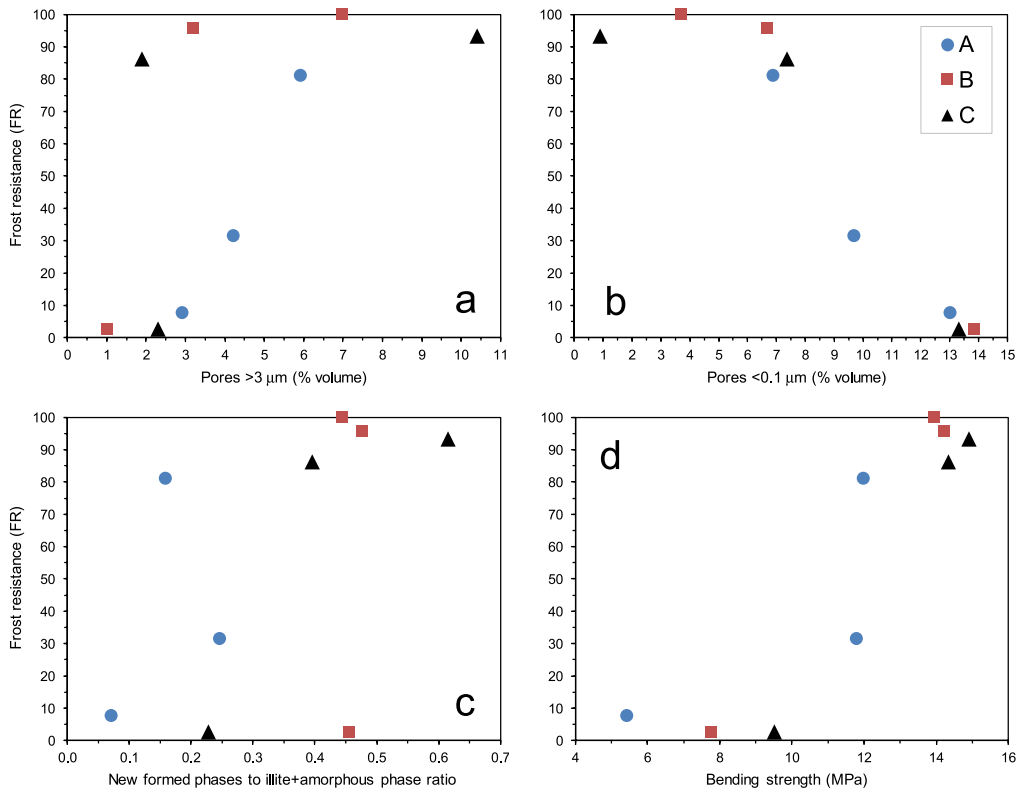

Fig. 8. Frost resistance of roof tiles as a function of the amount of pores >3 μm (a) or pores <0.1 μm (b), phase composition (c), and bending strength (d).

- It is possible to obtain an excellent resistance to freeze-thaw cycles even in presence of carbonates;
- Unlike current prediction schemes, the frost resistance depends on both pore size (in particular the pore fraction <0.1 μm) and degree of sintering (especially the bending strength); excellent frost resistance is achieved when pores <0.1 μm disappear and the flexural modulus of rupture is greater than 13 MPa).

The challenge of developing a predictive tool for the frost resistance of roof tiles, based on pore structure, phase composition and mechanical performance, is still open.

Declaration of competing interest

The authors declare that they have no known competing financial interests or personal relationships that could have appeared to influence the work reported in this paper.

Acknowledgements

The authors are grateful to CertiMac Faenza (Italy) and in particular to Marco Marsigli for carrying out the frost resistance and mechanical tests.

References

[1] M. Nakamura, Indirect evaluation of frost susceptibility of building materials, Am. Ceram. Soc. Bull. 67 (12) (1988) 1664–1965.
[2] W. Hansen, J.H. Kung, Pore structure and frost durability of clay bricks, Mater. Struct. 21 (1988) 443–447.
[3] M. Šveda, Frost resistance of brick, Am. Ceram. Soc. Bull. 80 (9) (2001) 46–48.
[4] G. Wardeh, B. Perrin, Freezing–thawing phenomena in fired clay materials and consequences on their durability, Construct. Build. Mater. 22 (2008) 820–828.
[5] M. Raimondo, C. Ceroni, M. Dondi, G. Guarini, M. Marsigli, I. Venturi, C. Zanelli, Durability of clay roofing tiles: the influence of microstructural and compositional variables, J. Eur. Ceram. Soc. 29 (2009) 3121–3128.
[6] I.N. Grubeša, M. Vračević, J. Ranogajec, V. Vučetić, Infuence of pore-size distribution on the resistance of clay brick to freeze-thaw cycles, Materials 13 (10) (2020) 2364.
[7] M. Šveda, Effect of water absorption on frost resistance of clay roofing tiles, Br. Ceram. Trans. 102 (2003) 43–45.
[8] P. Vincenzini, Le prove di laboratorio nella previsione del comportamento al gelo dei materiali ceramici per l'edilizia, Ceramurgia 3 (1974) 176–188.
[9] M. Maage, Frost resistance and pore size distribution in bricks, Part 1 Ziegelindustrie Int. 9 (1990) 472–481.
[10] M. Maage, Frost resistance and pore size distribution in bricks, Part 2 Ziegelindustrie Int. 10 (1990) 582–588.
[11] M. Arnott, Investigation of freeze-thaw durability, in: NRC-IRC Report N. CR 5680.1, Nat. Res. Council of Canada, Ottawa, Canada, 1990.
[12] L. Franke, H. Bentrup, Evaluation of the frost resistance of bricks in regard to long service life, Part 1 Ziegelindustrie Int. 7–8 (1993) 483–492.
[13] L. Franke, H. Bentrup, Evaluation of the frost resistance of bricks in regard to long service life, Part 2 Ziegelindustrie Int. 9 (1993) 528–536.
[14] G.C. Robinson, Relation between physical properties and durability of commercial marketed bricks, Am. Ceram. Soc. Bull. 56 (12) (1995) 1071–1075.
[15] R. Koroth, P. Fazio, D. Fedman, Comparative study of durability indices of clay bricks, J. Architect. Eng. 9 (1) (1998) 26–33.
[16] R. Koroth, P. Fazio, D. Fedman, Development of new durability index for clay bricks, J. Architect. Eng. 9 (1988) 87–93.
[17] T. Stryszewska, S. Kańka, Forms of damage of bricks subjected to cyclic freezing and thawing in actual conditions, Materials 12 (7) (2019) 1165.
[18] I. Netinger, M. Vracevic, J. Ranogajec, S. Vucetic, Evaluation of brick resistance to freeze/thaw cycles according to indirect procedures, Gradjevinar 66 (2014) 197–209.
[19] M. Sveda, M. Kerestur, R. Sokolar, L. Nevrivova, S. Uncik, Determination of suitable raw materials for preparation of frost resistant brick body and its evaluation according to pore size distribution, J. Ceram. Soc. Jpn. 123 (2015) 1441.
[20] A. Escardino, V. Beltrán, A. Barba, E. Sánchez, Liquid suction by porous ceramic materials. 4. Influence of firing conditions, Br. Ceram. Trans. J. 98 (5) (1999) 225–229.
[21] K. Ikeda, H.S. Kim, K.A. Kaizu Higashi, Influence of firing temperature on frost resistance of roofing tiles, J. Eur. Ceram. Soc. 24 (2004) 3671–3677.
[22] G. Cultrone, E. Sebastián, K. Elert, M.J. de la Torre, O. Cazalla, C. Rodriguez-Navarro, Influence of mineralogy and firing temperature on the porosity of bricks, J. Eur. Ceram. Soc. 24 (2004) p547–564.

[23] V. Ducman, S.A. Škapin, M. Radeka, J. Rnogajec, Frost resistance of clay roofing titles: case study, Ceram. Int. 37 (2011) 85–91.
[24] M. Šveda, R. Sokolář, The Effect of firing temperature on the irreversible expansion, water absorption and pore atructure of a brick body during freeze-thaw cycles, Mater. Sci. 19 (4) (2013).
[25] K. Elert, G. Cultrone, C. Rodriguez, N.E.S. Pardo, Durability of bricks used in the conservation of historic buildings — influence of composition and microstructure, J. Cult. Herit. 4 (2) (2003) 91–99.
[26] S. Freyburg, A. Schwarz, Influence of the clay type on the pore structure of structural ceramics, J. Eur. Ceram. Soc. 27 (2006) 1727–1733.
[27] I.A. Ivleva, O.A. Panova, Comprehensive evaluation of the effect of the mineralogical composition of clays and a porous glass component on the thermal conductivity and frost resistance of the heat-efficient wall ceramics, Glass Ceram. 76 (2019) 297–301.
[28] Cerame-Unie, Ceramic Roadmap to 2050: Continuing Our Path towards Climate Neutrality, The European Ceramic Industry Association, 2021, p. 72.
[29] T. Ros-Dosdá, P. F-i-Palmer, A. Mezquita, P. Masoni, E. Monfort, How can the European ceramic tile industry meet the EU's low-carbon targets? A life cycle perspective, J. Clean. Prod. 199 (2018) 554–564.
[30] I.N. Grubeša, M. Vračević, V. Ducman, B. Marković, I. Szenti, A. Kukovecz, Infuence of pore-size distribution on the resistance of clay brick to freeze-thaw cycles, Materials 13 (17) (2020) 3717.
[31] T. Stryszewska, S. Kańka, Characterization of factors determining the durability of brick masonry, in: Brick and Block Masonry - from Historical to Sustainable Masonry, 2020. Reference to a chapter in an edited book.
[32] M. Dondi, G. Ercolani, B. Fabbri, G. Guarini, M. Marsigli, C. Mingazzini, Major deposits of brick clays in Italy. Part 1: geology and composition [4], Tile & Brick Int 15 (1999) 230–237. Part 2: Technological properties and uses. Tile & Brick Int., 15, 5, (1999) 360-370.
[33] M. Dondi, Clay materials for ceramic tiles from the Sassuolo District (northern Apennines, Italy). Geology, composition and technological properties, Appl. Clay Sci. 15 (1999) 337–366.
[34] A.F. Gualtieri, Accuracy of XRPD QPA using the combined Rietveld_RIR method, J. Appl. Crystallogr. 33 (2000) 267–278.
[35] D.A. Quenard, K. Xu, H.M. Kiinzel, D.P. Bentz, N.S. Martys, Microstructure and transport properties of porous building materials, Mater. Struct./Mater. Construct. 31 (1998) 317–324.
[36] S. Freyburg, A. Schwarz, Influence of the clay type on the pore structure of structural ceramics, J. Eur. Ceram. Soc. 27 (2006) 1727–1733.
[37] N. Grubeša, M. Benšić, M. Vračević, New methods for assessing brick resistance to freeze-thaw cycles, Mater. Construcción 71 (2021) e258.